helicase inhibitors could be potential therapeutic agents. However, no HCV NS3 helicase inhibitors have yet been entered into clinical trials, at least in part due to similarities between NS3 and cellular RNA helicases [8].

HCV NS3 helicase is part of the family of viral DExH proteins; the NS3/NPH-II family that encompasses helicases from positive-stranded RNA viruses [16–18]. These closely related helicases share a catalytic core that consists mainly of NTPase and nucleic acid binding sites, as well as many other structural and functional features. Indeed, dengue virus (DENV) NS3 helicase, another viral DExH protein, and HCV NS3 helicase share highly conserved amino acid sequences, and consequently have similar conformational structures [19]. Thus, if a compound inhibits HCV NS3 helicase, it may also inhibit DENV NS3 helicase [20–22]. Assessing the inhibitory specificity can provide useful information to understand whether inhibitors target the NTPase, nucleic acid binding, or other allosteric sites of NS3 helicase.

HCV NS3 helicase inhibitors function by inhibiting NTP binding, nucleic acid binding, NTP hydrolysis or NDP release, the coupling of NTP hydrolysis to the translocation and unwinding of nucleic acids, or unwinding by sterically blocking helicase translocation [6]. In addition, owing to an interdependent linkage between NS3 helicase and serine protease activities [23–25], the inhibition of NS3 serine protease may also lead to the inhibition of NS3 helicase. Compounds that intercalate into the strands of double-stranded nucleic acids could also inhibit NS3 helicase [26].

Naturally occurring products are an important source of structurally diverse and biologically active secondary metabolites. The diversity of organisms in the marine environment has provided new drugs in almost all therapeutic areas [27–29]. To date, seven therapeutic agents derived from the marine environment are used as anticancer, antiviral, pain control, and hypertriglyceridemia agents [27]. The chemical structure has been isolated for two of these compounds, whereas the remaining five are synthetic agents based on marine products. An additional 13 agents are in phase 1, 2, or 3 clinical trials. Therefore, natural marine products include a number of highly significant lead compounds that are driving new drug development.

In this study, we screened extracts from marine organisms for NS3 helicase inhibitors using a fluorescence helicase assay based on photoinduced electron transfer (PET), as described in our previous study [30]. During purification, halisulfate 3 (hal3) and suvanine, which were isolated from marine sponge extracts, were identified as novel NS3 helicase inhibitors with IC_{50} values in the low micromolar range. The inhibitory effects of hal3 and suvanine against the other helicase-related activities of NS3 (ATPase, RNA binding, and serine protease activities) were also assessed. Finally, the inhibitory activities of hal3 and suvanine against DENV NS3 helicase were determined to characterize the binding sites of hal3 and suvanine.

2. Results and Discussion

To obtain novel NS3 helicase inhibitors, extracts from marine organisms were screened using a fluorescence helicase assay based on PET. Forty-three extracts prepared from marine organisms were screened, and 11 were identified that inhibited the helicase activity >50% (samples 4, 10, 13, 14, 17, 19, 21, 22, 25, 26, and 37) (Table 1), suggesting that these extracts contained NS3 helicase inhibitors. Of these extracts, sample 10 exhibited the strongest inhibition of NS3 helicase, and abolished its

activity completely. Therefore, this extract was purified to isolate and concentrate the inhibitory components. After several purification steps, the inhibitory components were identified as hal3 and suvanine (Figure 1) by comparing their NMR spectra with those reported previously [31,32] for each compound (Supplementary Figures S1–S4). Hal3 and suvanine inhibited NS3 helicase activity in a dose-dependent manner, with IC_{50} values of 4 and 3 μM, respectively (Figure 2A,B).

Table 1. Inhibitory effects of extracts from marine organisms on hepatitis C virus (HCV) nonstructural protein 3(NS3) helicase activity.

No.	NS3 Helicase Activity (% of Control) *	Marine Organism	Species
1	92	Sponge	*Unidentified*
2	74	Soft coral	*Briareum*
3	57	Tunicate	*Unidentified*
4	36	Sponge	*Liosina*
5	54	Sponge	*Unidentified*
6	71	Sponge	*Xestospongia*
7	77	Sponge	*Epipolasis*
8	110	Sponge	*Unidentified*
9	86	Sponge	*Strongylophora*
10	**0**	**Sponge**	***Unidentified***
11	83	Sponge	*Stylotella aurantium*
12	78	Sponge	*Epipolasis*
13	25	Sponge	*Unidentified*
14	43	Sponge	*Hippospongia*
15	75	Sponge	*Unidentified*
16	85	Sponge	*Unidentified*
17	49	Sponge	*Xestospongia testudinaria*
18	69	Sponge	*Unidentified*
19	40	Sponge	*Theonella*
20	64	Sponge	*Unidentified*
21	44	Sponge	*Unidentified*
22	46	Sponge	*Petrosia*
23	72	Tunicate	*Unidentified*
24	61	Sponge	*Unidentified*
25	50	Tunicate	*Didemnum molle*
26	33	Sponge	*Unidentified*
27	67	Sponge	*Unidentified*
28	87	Soft coral	*Unidentified*
29	62	Sponge	*Unidentified*
30	60	Sponge	*Unidentified*
31	85	Sponge	*Cinachyra*
32	70	Sponge	*Liosina*
33	68	Sponge	*Unidentified*
34	58	Sponge	*Unidentified*
35	72	Sponge	*Stylotella*
36	57	Sponge	*Unidentified*
37	39	Sponge	*Unidentified*

Table 1. *Cont.*

38	72	Tunicate	*Didemnum*
39	62	Sponge	*Unidentified*
40	71	Jellyfish	*Unidentified*
41	74	Sponge	*Unidentified*
42	52	Tunicate	*Unidentified*
43	67	Annelid	*Unidentified*

* NS3 helicase activity in the presence of extract is expressed as a percentage of control in the absence of extract (100%); The sample with the strongest inhibition against NS3 helicase is in bold, underlined font; samples with relatively strong inhibition against NS3 helicase (<50%) are underlined.

Figure 1. Structures of halisulfate 3 (hal3) and suvanine.

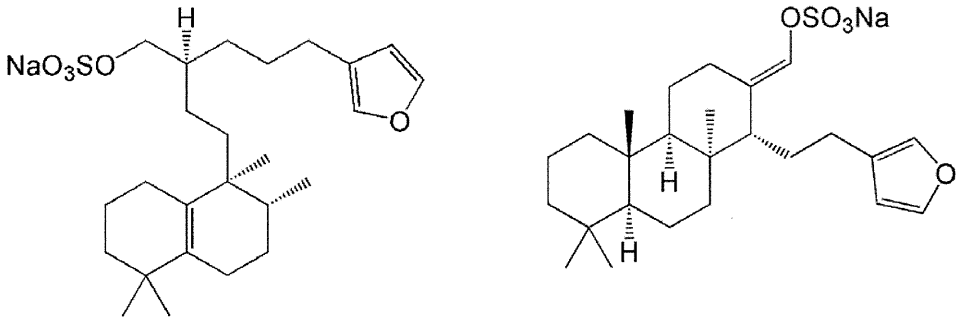

Halisulfate 3 Suvanine

The inhibitory effects of hal3 and suvanine were confirmed using a gel-based helicase assay. The helicase activity was calculated as the ratio of the signal intensity derived from single-stranded (ssRNA) in the sample containing the inhibitor to the control sample (lacking the inhibitor but containing DMSO vehicle). Similar to the results of the fluorescence helicase assay, hal3 and suvanine inhibited helicase-catalyzed RNA unwinding in a dose-dependent manner (Figure 2C,D). Therefore, these data clearly indicate that hal3 and suvanine exert inhibitory effects. Hal3 and suvanine were identified in 1988 [33] and 1985 [34], respectively. They have similar distinguishing structural features of a sulfated side chain and a furan moiety at the terminus of the molecule (Figure 1). Although some bioactivities for hal3 and suvanine have been reported, this report is the first that identifies these compounds as helicase inhibitors. In addition, bioactive effects of hal3 alone have not been reported. A mixture of halisulfates 2–5 (hal3 and its analogues) showed antimicrobial activity against *S. aureus*, *C. albicans*, and *B. subtilis*. Moreover, a mixture of halisulfates 2–4 inhibited PMA-induced inflammation in a mouse ear edema assay and inhibited phospholipase A_2 [31]. Suvanine is a serine protease inhibitor [35] and an antagonist of the mammalian bile acid sensor farnesoid-X-receptor [36]. In addition, suvanine interferes with heat shock protein 60, a chaperone involved in the inflammatory response, giving evidence for its anti-inflammatory properties [37].

Figure 2. Inhibition of NS3 helicase-catalyzed RNA unwinding activity by hal3 and suvanine. (**A**,**B**) Inhibition curves of hal3 and suvanine generated using a fluorescence helicase assay. The NS3 helicase activities of samples containing inhibitor were calculated relative to control samples containing DMSO vehicle rather than inhibitor. The data are presented as mean ± standard deviation of three replicates; (**C**,**D**) Gel images representing the inhibitory effects of hal3 and suvanine in a gel-based helicase assay. Fluorescence-labeled ssRNA and dsRNA were applied to lanes *1* and *2*, respectively. The dsRNA was incubated with NS3 in the presence of increasing concentrations of inhibitor (lanes *3*–*7*, 0–100 μM). Lane *8* shows the control reaction in the absence of NS3.

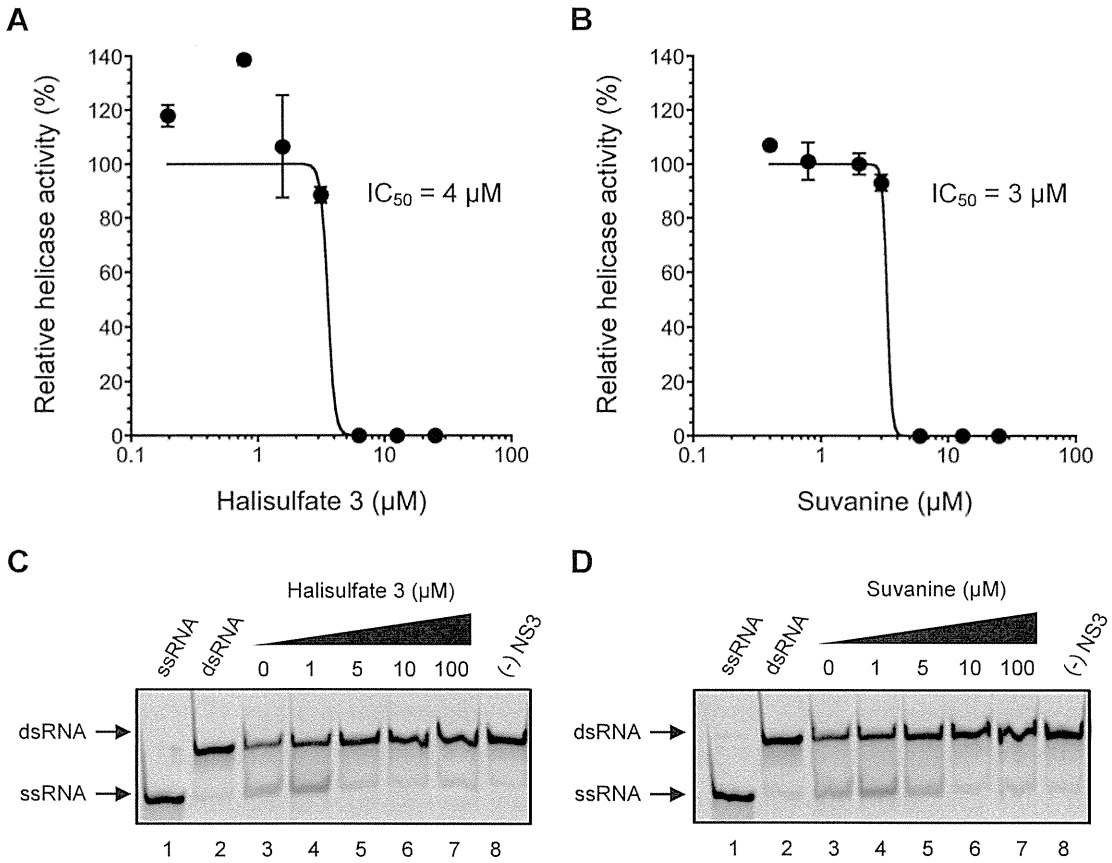

As the unwinding ability of NS3 helicase is dependent on ATP hydrolysis, the amount of inorganic phosphate (Pi) released from radioisotope-labeled ATP was measured to determine the effects of hal3 and suvanine on the ATPase activity of NS3 (Figure 3). The released Pi was separated by thin-layer chromatography and visualized using autoradiography. The density of the upper spots corresponding to Pi, which represents ATPase activity, decreased dose-dependently for both hal3 and suvanine. The ATPase activity was calculated as the ratio of the signal intensity derived from the released Pi in the sample containing inhibitor to that in the control sample (lacking the inhibitor but containing DMSO vehicle). The IC_{50} values of hal3 and suvanine were calculated to be 8 and 7 μM, respectively. As this concentration range is similar to that in which RNA unwinding was inhibited (Figure 2), it is likely that hal3 and suvanine inhibit NS3 helicase via the inhibition of ATPase activity.

Figure 3. Effects of hal3 and suvanine on NS3 ATPase activity demonstrated by autoradiography of an ATPase assay using [γ-^{32}P] ATP. Lane *1* contains the control reaction without NS3. Lanes *2–8* (**A**) and *2–9* (**B**) show the ATP hydrolysis reaction with poly(U) RNA at increasing concentrations (0–100 μM) of hal3 and suvanine, respectively.

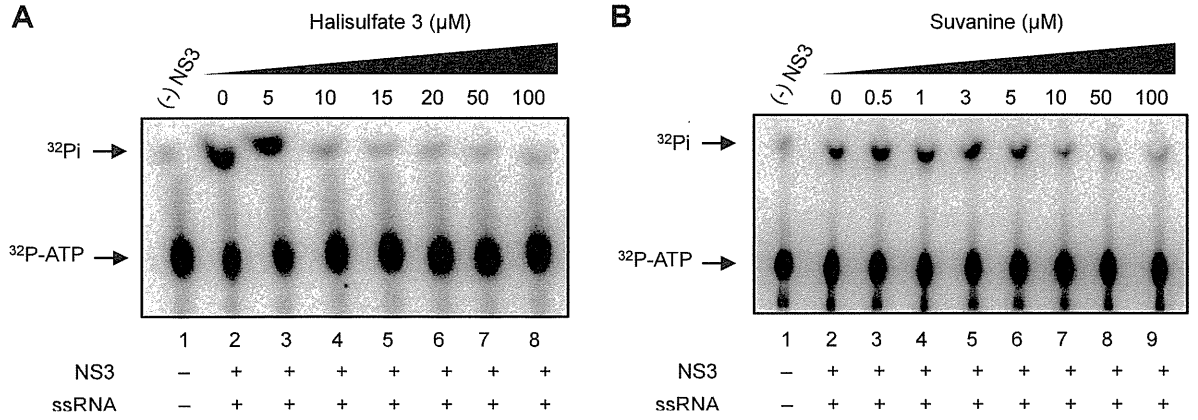

As RNA binding is required for NS3 helicase activity, the effects of hal3 and suvanine on NS3 RNA binding activity were examined by gel mobility shift assay (Figure 4). As a control, the non-specific binding of ssRNA to bovine serum albumin (BSA) was assessed (lane 2). The density of the upper bands corresponding to the NS3-ssRNA complex, which represents NS3 RNA binding activity, decreased dose-dependently in the presence of both hal3 and suvanine. RNA binding activity was calculated as the ratio of the signal intensity derived from the NS3-ssRNA complex in the sample containing the inhibitor to that in the control sample (lacking the inhibitor but containing DMSO vehicle). The IC_{50} values of hal3 and suvanine were calculated to be 8 and 3 μM, respectively. The data presented in Figures 2 and 4 reveal that the NS3 helicase and RNA binding activities decrease at similar inhibitor concentration ranges for hal3 and suvanine, suggesting that the inhibition of NS3 helicase by these compounds is associated with RNA binding activity.

Figure 4. Effects of hal3 and suvanine on NS3 RNA binding activity, assessed by autoradiography of a gel mobility shift assay using ^{32}P-labeled ssRNA. Lanes *1* and *2* contain control reactions consisting of heat-denatured ssRNA and 300 nM BSA instead of NS3, respectively. Lanes *3–9* (**A**) and *3–10* (**B**) show the RNA binding reaction with increasing concentrations (0–100 μM) of hal3 and suvanine, respectively.

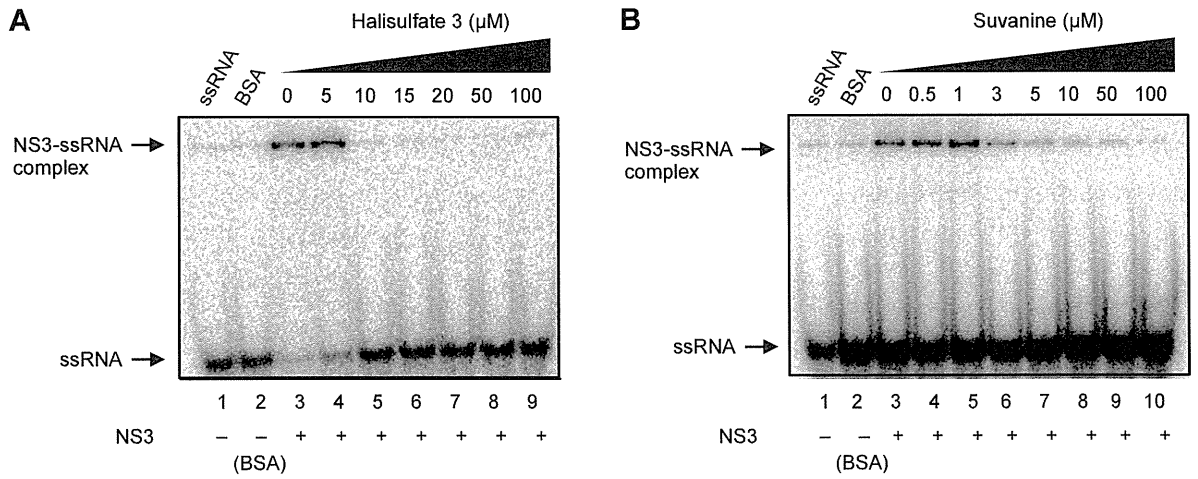

It was reported that the helicase activity of NS3 is interdependently linked to its serine protease activity [23–25]. Therefore, we examined the effects of hal3 and suvanine on NS3 serine protease activity using a fluorescence serine protease assay (Figure 5). Serine protease activity decreased in a dose-dependent manner in the presence of hal3 and suvanine, with IC_{50} values of 14 and 34 μM, respectively. Although the inhibition of the serine protease activity seems to be rather modest compared with that of the ATPase and RNA binding activities (Figures 3 and 4), the inhibition of NS3 helicase by hal3 and suvanine is likely to be also related to serine protease activity.

Figure 5. Effects of hal3 (**A**) and suvanine (**B**) on NS3 serine protease activity. The NS3 serine protease activity of samples containing inhibitor was calculated relative to control samples containing DMSO vehicle rather than inhibitor. The data are presented as means ± standard deviation of three replicates.

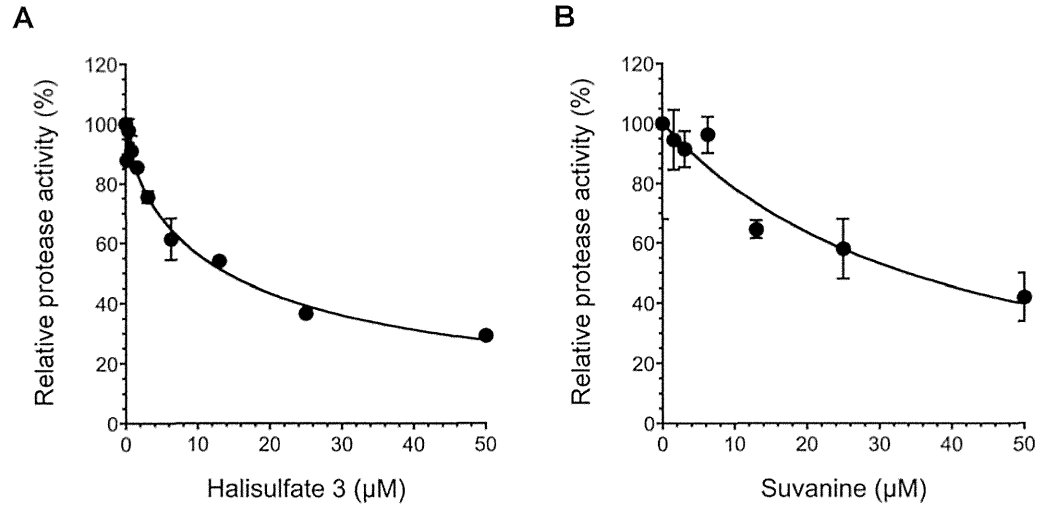

The catalytic cores of DENV and HCV NS3 helicases, which consist predominantly of ATPase and RNA binding sites, share almost identical folds and extensive structural similarity [38]. Because the substrate specificity of DENV and HCV NS3 helicases is similar [39], the dsRNA substrate and capture strand of the gel-based HCV NS3 helicase assay were also used for the gel-based DENV NS3 helicase assay (Figure 6), and helicase activity was calculated as described above. Hal3 and suvanine did not abolish DENV NS3 helicase activity, even in the presence of 100 μM of each inhibitor. This finding suggests that the inhibitory effects of hal3 and suvanine are specific to HCV NS3 helicase, and that these inhibitors bind less efficiently to any site in DENV NS3 helicase, including the catalytic core.

This study demonstrated that hal3 and suvanine inhibit the ATPase, RNA binding, and serine protease activities of NS3 (Figures 3–5). Taken together with observations that hal3 and suvanine did not inhibit DENV NS3 helicase (Figure 6), it is likely that these inhibitors do not bind to the catalytic core that contains the ATPase activity and RNA binding sites. Therefore, we conclude that hal3 and suvanine inhibit HCV NS3 helicase via interactions with allosteric sites of NS3. This likely induces conformational changes in NS3, inhibiting or abolishing its activities. Compounds with inhibitory activities against both helicase and serine protease activities have been reported previously [40]; however, there are only a small number of studies, and detailed inhibitory mechanisms are yet to be elucidated. The possible allosteric sites to which hal3 and suvanine bind could be an interface that

forms between the helicase and protease domains of NS3. Indeed, a novel small-molecule binding site at the interface between these two domains was reported recently [41]. Furthermore, the inhibitory specificity of hal3 and suvanine against HCV NS3 helicase might be explained by structural differences between HCV and DENV NS3 helicases. A specific beta-strand tethers the *C* terminus of the helicase domain to the protease domain of HCV NS3, maintaining it in a compact conformation that differs from the extended conformation of DENV NS3 helicase [42]. As only HCV NS3 helicase forms an interface between the helicase and protease domains, the specificity of hal3 and suvanine for HCV NS3 helicase would be explained by the binding of hal3 and suvanine to the interface of HCV NS3.

Figure 6. Effects of hal3 (**A**) and suvanine (**B**) on DENV NS3 helicase activity, assessed using a gel-based helicase assay. Fluorescence-labeled ssRNA and dsRNA were applied to lanes *1* and *2*, respectively. The dsRNA was incubated with NS3 in the presence of increasing concentrations of inhibitor (lanes *3*–*7*, 0–100 μM). Lanes *8* and *9* contain the control reaction mixtures in the absence of NS3, and in the presence of 15 mM ATP-gamma-S as an inhibition control, respectively.

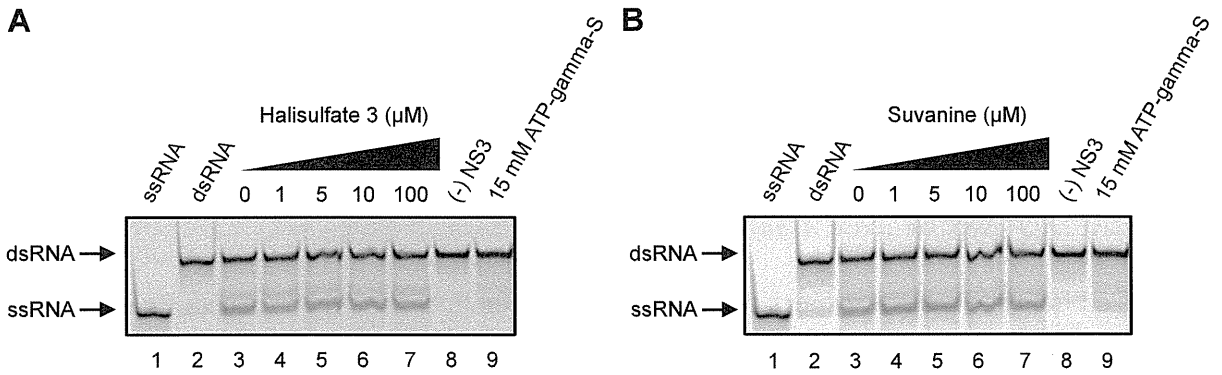

3. Experimental Section

3.1. Preparation of Extracts from Marine Organisms

Specimens of marine organisms were collected by scuba diving in Okinawa, Japan, and Sorong, Indonesia, and kept frozen until use. The specimens were chopped into small pieces, and soaked in acetone for 20 h followed by methanol for 6 h. The acetone and methanol solutions were then combined and concentrated, and residual materials were separated into ethyl acetate and aqueous layers; each layer was then dried to obtain residues.

3.2. Screening for HCV NS3 Helicase Inhibitors

The PET-based fluorescence helicase assay was performed as described previously [30]. The dsRNA substrate was prepared by annealing the 5′ BODIPY FL-labeled fluorescence strand (5′-CUAUUACCUCCACCCUCAUAACCUUUUUUUUUUUUUU-3′) to the quencher strand (5′-GGUUAUGAGGGUGGAGGUAAUAG-3′) at a 1:2 molar ratio. The dsRNA substrate contains the 3′-overhang that is necessary for the NS3 helicase to bind RNA prior to duplex unwinding. The capture strand (5′-CTATTACCTCCACCCTCATAACC-3′), which is complementary to the quencher strand, prevents the unwound duplexes from reannealing. None of the capture, quencher, or fluorescence

strands are self-complementary. The fluorescence strand was purchased from J-Bio 21 Corporation (Tokyo, Japan), and was labeled with BODIPY FL at the 5′-end via an aminohexylphosphate linker with a six-carbon spacer. The quencher and capture strands were purchased from Japan Bio Services (Saitama, Japan). The reaction mixture contained 25 mM MOPS-NaOH (pH 6.5), 3 mM $MgCl_2$, 2 mM dithiothreitol, 4 U RNasin (Promega, Madison, WI, USA), 50 nM dsRNA substrate, 100 nM capture strand, 5 mM ATP, a marine organism extract, and 240 nM NS3 in a total reaction volume of 20 μL. Each marine organism extract diluted in DMSO was added to the reaction mixture at a final concentration of 17.5–32.5 μg/mL. The full-length HCV NS3 protein with serine protease and NTPase/helicase activities was expressed and purified as described previously [43].

The reaction was started by the addition of HCV NS3 helicase, and was performed at 37 °C for 30 min using a LightCycler 1.5 (Roche Diagnostics, Basel, Switzerland). The fluorescence intensity was recorded every 5 s from 0 to 5 min, and then every 30 s from 5 to 30 min. Helicase activity was calculated as the initial reaction velocity relative to control (in the absence of a marine extract, but presence of DMSO vehicle). The IC_{50} was calculated using KaleidaGraph (Synergy Software, Reading, PA, USA) by fitting plots of % activity *vs.* [*I*] using Equation (1) unless otherwise noted [44]:

$$\% \text{ Activity} = \frac{100}{1+\left([I]/\text{IC}_{50}\right)^{h}} \quad (1)$$

where *h* is the Hill coefficient, and [*I*] is the inhibitor concentration.

3.3. Gel-Based HCV NS3 Helicase Assay

A gel-based helicase assay was performed on HCV NS3 helicases using an Alexa Fluor 488-labeled dsRNA strand and capture strand with the same nucleic acid sequences described in Section 3.2. The dsRNA substrate was prepared by annealing the 5′ Alexa Fluor 488-labeled strand (5′-CUAUUACCUCCACCCUCAUAACCUUUUUUUUUUUUUU-3′) to the complementary strand (5′-GGUUAUGAGGGUGGAGGUAAUAG-3′) at a 1:2 molar ratio. The same capture strand described in Section 3.2 was used. All nucleic acid strands were purchased from Japan Bio Services (Saitama, Japan). The reaction mixture for HCV NS3 helicase contained the same components as described in Section 3.2, with increasing concentrations of hal3 or suvanine in a reaction volume of 20 μL. The reaction was started by the addition of HCV NS3 helicase, and performed at 37 °C for 60 min using a GeneAmp PCR System 2700 (Applied Biosystems, Foster City, CA, USA). The reaction was stopped by the addition of 5 μL of helicase termination buffer containing 10 mM Tris-HCl (pH 7.5), 50 mM EDTA, 30% glycerol, 0.06% bromophenol blue, and 0.12% Orange G. The inhibition of NS3 helicase was analyzed on a 20% native Tris/borate/EDTA (TBE) polyacrylamide gel, and labeled RNAs were visualized using Typhoon 9210 (GE Healthcare, Waukesha, WI, USA). The helicase activity was calculated as the ratio of the signal intensity derived from ssRNA in the sample containing inhibitor to that in the control sample containing DMSO vehicle instead of inhibitor.

3.4. ATPase Assay

NS3 ATPase activity was determined directly by monitoring [γ-^{32}P] ATP hydrolysis by thin-layer chromatography, as described previously [45,46]. The reaction mixture contained 25 mM MOPS-NaOH

(pH 7.0), 1 mM dithiothreitol, 5 mM $MgCl_2$, 5 mM $CaCl_2$, 1 mM [γ-^{32}P] ATP (Muromachi Yakuhin, Tokyo, Japan), 300 nM NS3, 0.1 μg/μL poly (U) ssRNA (Sigma-Aldrich, St. Louis, MO, USA), and increasing concentrations of hal3 or suvanine in a volume of 10 μL. The reaction was conducted at 37 °C for 10 min, and stopped by the addition of 10 mM EDTA. Two microliters of each reaction mixture was then spotted onto a polyethyleneimine cellulose sheet (Merck, Darmstadt, Germany) and developed in 0.75 M LiCl/1 M formic acid solution for 20 min. The cellulose sheet was dried, and the released [γ-^{32}P] phosphoric acid was visualized using an Image Reader FLA-9000 and quantified using Multi Gauge software V 3.11 (Fujifilm, Tokyo, Japan). ATPase activity was calculated as the ratio of the signal intensity derived from the released Pi in the sample containing inhibitor to that in the control sample containing DMSO vehicle instead of inhibitor.

3.5. RNA Binding Assay

NS3 RNA binding activity was determined by gel mobility shift assay, as described previously [45,46]. The ssRNA (5′-UGAGGUAGUAGGUUGUAUAGU-3′) synthesized by Gene Design (Osaka, Japan) was labeled at the 5′-end with [γ-^{32}P] ATP (Muromachi Yakuhin, Tokyo, Japan) using T4 polynucleotide kinase (Toyobo, Osaka, Japan) at 37 °C for 60 min, and purified using the phenol-chloroform extraction method. The reaction mixture contained 30 mM Tris-HCl (pH 7.5), 100 mM NaCl, 2 mM $MgCl_2$, 1 mM dithiothreitol, 20 U RNasin Plus (Promega), 300 nM NS3, 0.1 nM ^{32}P-labeled ssRNA, and increasing concentrations of inhibitor in a volume of 20 μL. The reaction was performed at room temperature for 15 min. An equal volume of a dye solution containing 0.025% bromophenol blue and 10% glycerol in 0.5× TBE was then added to each reaction mixture, and samples were loaded onto a 6% native-polyacrylamide gel. The labeled RNA bands were visualized using an Image Reader FLA-9000 and quantified using Multi Gauge software V 3.11 (Fujifilm, Tokyo, Japan). RNA binding activity was calculated as the ratio of the signal intensity derived from the NS3-ssRNA complex in the sample containing hal3 or suvanine to that in the control sample containing DMSO vehicle rather than inhibitor.

3.6. Serine Protease Assay

A fluorescence NS3 serine protease assay, based on fluorescence resonance energy transfer, was conducted using reagents provided in a SensoLyte™ 520 HCV protease assay kit (AnaSpec, San Jose, CA, USA), as described previously [30]. Briefly, NS3 protein with a two-fold excess of the NS4A cofactor peptide Pep4AK was prepared in 1× assay buffer provided with the kit. HCV NS3/4A protease was mixed with increasing concentrations of inhibitor, and incubated at 37 °C for 15 min. The reaction was started by the addition of 5-FAM/QXL 520 substrate in a 20 μL total reaction volume containing 240 nM HCV NS3/4A protease and increasing concentrations of hal3 or suvanine. Reactions were then incubated at 37 °C for 120 min on a LightCycler 1.5 (Roche Diagnostics, Basel, Switzerland), and the fluorescence intensity was recorded every min for 120 min. NS3 serine protease activity was calculated as the initial reaction velocity in the sample containing inhibitor relative to the control sample containing DMSO vehicle rather than inhibitor.

3.7. Gel-Based DENV NS3 Helicase Assay

A gel-based helicase assay was performed using DENV NS3 helicases, and the Alexa Fluor 488-labeled dsRNA strand and capture strand with the same nucleic acid sequences described in the Section 3.3. DENV NS3 helicase requires a single stranded 3′ overhang to unwind dsRNA substrates in the 3′ to 5′ direction [39]; therefore, the substrate specificities of the DENV and HCV NS3 helicases are the same. The reaction mixture contained 50 mM Tris-HCl (pH 7.4), 1 mM DTT, 0.5% Tween 20, 0.25 μg/mL BSA, 2 mM $MgCl_2$, 4 U RNasin (Promega), 5 mM ATP, 50 nM dsRNA substrate, 300 nM capture strand, an inhibitor, and 240 nM DENV NS3 in a total volume of 20 μL. DENV NS3 helicase was prepared as described previously [47]. The reaction was started by the addition of DENV NS3 helicase, and was performed at 37 °C for 60 min using a GeneAmp PCR System 2700 (Applied Biosystems, Foster City, CA, USA). The reaction was then stopped by the addition of 5 μL helicase termination buffer that contained 10 mM Tris-HCl (pH 7.5), 50 mM EDTA, 30% glycerol, 0.06% bromophenol blue, and 0.12% Orange G. The inhibition of DENV NS3 helicase was analyzed on a 20% native TBE polyacrylamide gel, and the labeled RNAs were visualized using Typhoon 9210 (GE Healthcare, Waukesha, WI, USA). The helicase activity was calculated as the ratio of the signal intensity from ssRNA in the sample containing inhibitor to that in the control sample containing DMSO vehicle instead of inhibitor.

4. Conclusions

This study demonstrated that hal3 and suvanine isolated from a marine sponge inhibited NS3 helicase by suppressing the ATPase, RNA binding, and serine protease activities. Moreover, DENV NS3 helicase, which shares a catalytic core consisting mainly of ATPase and RNA binding activity sites with HCV NS3 helicase, was not inhibited by hal3 or suvanine. Therefore, it can be concluded that hal3 and suvanine inhibit HCV NS3 helicase specifically through interaction with an allosteric site of NS3 rather than the catalytic core, leading to the inhibition of all NS3 activities, presumably by inducing conformational changes. As such, it is possible that hal3 and suvanine are less likely to inhibit other cellular helicases that share a similar catalytic core to HCV NS3 helicase. This provides potentially useful information on advanced drug design strategies to identify novel NS3 helicase inhibitors that are expected to be more specific and less toxic. Experiments to address whether resistant HCV mutants emerge with the use of these compounds are underway in our laboratory.

Acknowledgments

The authors thank S. Nishikawa (AIST) for his kind gift of the expression plasmid pT7/His-NS3 containing the *N*-terminal His-tagged full-length HCV NS3. The Global COE Program "Center for Practical Chemical Wisdom" of the Ministry of Education, Culture, Sports, Science and Technology (MEXT) of Japan partially supported this study. This work was also partly supported by NUS SoM Start-up Grant (R-182-000-160-733, R-182-000-160-133) to NY.

Conflicts of Interest

The authors declare no conflict of interest.

References

1. Ghany, M.G.; Nelson, D.R.; Strader, D.B.; Thomas, D.L.; Seeff, L.B. An update on treatment of genotype 1 chronic hepatitis C virus infection: 2011 practice guideline by the American Association for the Study of Liver Diseases. *Hepatology* **2011**, *54*, 1433–1444.
2. Liang, T.J.; Ghany, M.G. Current and future therapies for hepatitis C virus infection. *N. Engl. J. Med.* **2013**, *368*, 1907–1917.
3. Sarrazin, C.; Hézode, C.; Zeuzem, S.; Pawlotsky, J.-M. Antiviral strategies in hepatitis C virus infection. *J. Hepatol.* **2012**, *56*, S88–S100.
4. Scheel, T.K.H.; Rice, C.M. Understanding the hepatitis C virus life cycle paves the way for highly effective therapies. *Nat. Med.* **2013**, *19*, 837–849.
5. Lam, A.M.I.; Frick, D.N. Hepatitis C virus subgenomic replicon requires an active NS3 RNA helicase. *J. Virol.* **2006**, *80*, 404–411.
6. Kwong, A.D.; Rao, B.G.; Jeang, K.-T. Viral and cellular RNA helicases as antiviral targets. *Nat. Rev. Drug Discov.* **2005**, *4*, 845–853.
7. Bartenschlager, R.; Penin, F.; Lohmann, V.; André, P. Assembly of infectious hepatitis C virus particles. *Trends Microbiol.* **2011**, *19*, 95–103.
8. Bartenschlager, R.; Lohmann, V.; Penin, F. The molecular and structural basis of advanced antiviral therapy for hepatitis C virus infection. *Nat. Rev. Microbiol.* **2013**, *11*, 482–496.
9. Lohmann, V.; Körner, F.; Koch, J.-O.; Herian, U.; Theilmann, L.; Bartenschlager, R. Replication of subgenomic hepatitis C virus RNAs in a hepatoma cell line. *Science* **1999**, *285*, 110–113.
10. Gallinari, P.; Brennan, D.; Nardi, C.; Brunetti, M.; Tomei, L.; Steinkühler, C.; de Francesco, R. Multiple enzymatic activities associated with recombinant NS3 protein of hepatitis C virus. *J. Virol.* **1998**, *72*, 6758–6769.
11. Kim, D.W.; Gwack, Y.; Han, J.H.; Choe, J. *C*-terminal domain of the hepatitis C virus NS3 protein contains an RNA helicase activity. *Biochem. Biophys. Res. Commun.* **1995**, *215*, 160–166.
12. Tai, C.-L.; Chi, W.-K.; Chen, D.-S.; Hwang, L.-H. The helicase activity associated with hepatitis C virus nonstructural protein 3 (NS3). *J. Virol.* **1996**, *70*, 8477–8484.
13. Gwack, Y.; Kim, D.W.; Han, J.H.; Choe, J. Characterization of RNA binding activity and RNA helicase activity of the hepatitis C virus NS3 protein. *Biochem. Biophys. Res. Commun.* **1996**, *225*, 654–659.
14. Gwack, Y.; Kim, D.W.; Han, J.H.; Choe, J. DNA helicase activity of the hepatitis C virus nonstructural protein 3. *Eur. J. Biochem.* **1997**, *250*, 47–54.
15. Kolykhalov, A.A.; Mihalik, K.; Feinstone, S.M.; Rice, C.M. Hepatitis C virus-encoded enzymatic activities and conserved RNA elements in the 3′ nontranslated region are essential for virus replication *in vivo*. *J. Virol.* **2000**, *74*, 2046–2051.
16. Hall, M.C.; Matson, S.W. Helicase motifs: The engine that powers DNA unwinding. *Mol. Microbiol.* **1999**, *34*, 867–877.
17. Gorbalenya, A.E.; Koonin, E.V. Helicases: Amino acid sequence comparisons and structure-function relationships. *Curr. Opin. Struct. Biol.* **1993**, *3*, 419–429.
18. Jankowsky, E. *RNA Helicases*; Royal Society of Chemistry: London, UK, 2010; pp. 168–188.

19. Frick, D.N.; Lam, A.M.I. Understanding helicases as a means of virus control. *Curr. Pharm. Des.* **2006**, *12*, 1315–1338.
20. Borowski, P.; Deinert, J.; Schalinski, S.; Bretner, M.; Ginalski, K.; Kulikowski, T.; Shugar, D. Halogenated benzimidazoles and benzotriazoles as inhibitors of the NTPase/helicase activities of hepatitis C and related viruses. *Eur. J. Biochem.* **2003**, *270*, 1645–1653.
21. Zhang, N.; Chen, H.-M.; Koch, V.; Schmitz, H.; Liao, C.-L.; Bretner, M.; Bhadti, V.S.; Fattom, A.I.; Naso, R.B.; Hosmane, R.S.; *et al.* Ring-expanded ("fat") nucleoside and nucleotide analogues exhibit potent *in vitro* activity against *Flaviviridae* NTPases/helicases, including those of the West Nile virus, hepatitis C virus, and Japanese encephalitis virus. *J. Med. Chem.* **2003**, *46*, 4149–4164.
22. Borowski, P.; Heising, M.V.; Miranda, I.B.; Liao, C.-L.; Choe, J.; Baier, A. Viral NS3 helicase activity is inhibited by peptides reproducing the Arg-rich conserved motif of the enzyme (motif VI). *Biochem. Pharmacol.* **2008**, *76*, 28–38.
23. Frick, D.N.; Ginzburg, O.; Lam, A.M.I. A method to simultaneously monitor hepatitis C virus NS3 helicase and protease activities. *Methods Mol. Biol.* **2010**, *587*, 223–233.
24. Dahl, G.; Sandström, A.; Akerblom, E.; Danielson, U.H. Effects on protease inhibition by modifying of helicase residues in hepatitis C virus nonstructural protein 3. *FEBS J.* **2007**, *274*, 5979–5986.
25. Frick, D.N. The hepatitis C virus NS3 protein: A model RNA helicase and potential drug target. *Curr. Issues Mol. Biol.* **2007**, *9*, 1–20.
26. Belon, C.A.; Frick, D.N. Helicase inhibitors as specifically targeted antiviral therapy for hepatitis C. *Future Virol.* **2009**, *4*, 277–293.
27. Mayer, A.M.S.; Glaser, K.B.; Cuevas, C.; Jacobs, R.S.; Kem, W.; Little, R.D.; McIntosh, J.M.; Newman, D.J.; Potts, B.C.; Shuster, D.E. The odyssey of marine pharmaceuticals: A current pipeline perspective. *Trends Pharmacol. Sci.* **2010**, *31*, 255–265.
28. Gerwick, W.H.; Moore, B.S. Lessons from the past and charting the future of marine natural products drug discovery and chemical biology. *Chem. Biol.* **2012**, *19*, 85–98.
29. Newman, D.J.; Cragg, G.M. Natural products as sources of new drugs over the 30 years from 1981 to 2010. *J. Nat. Prod.* **2012**, *75*, 311–335.
30. Furuta, A.; Salam, K.A.; Akimitsu, N.; Tanaka, J.; Tani, H.; Yamashita, A.; Moriishi, K.; Nakakoshi, M.; Tsubuki, M.; Sekiguchi, Y.; *et al.* Cholesterol sulfate as a potential inhibitor of hepatitis C virus NS3 helicase. *J. Enzym. Inhib. Med. Chem.* **2013**, doi:10.3109/14756366.2013.766607.
31. Müller, E.L.; Faulkner, D.J. Absolute configuration of halisulfate 3 from the sponge *Ircinia* sp. *Tetrahedron* **1997**, *53*, 5373–5378.
32. Manes, L.V.; Crews, P.; Kernan, M.R.; Faulkner, D.J.; Fronczek, F.R.; Gandour, R.D. Chemistry and revised structure of suvanine. *J. Org. Chem.* **1988**, *53*, 570–575.
33. Kernan, M.R.; Faulkner, D.J. Sesterterpene sulfates from a sponge of the family Halichondriidae. *J. Org. Chem.* **1988**, *53*, 4574–4578.
34. Manes, L.V.; Naylor, S.; Crews, P.; Bakus, G.J. Suvanine, a novel sesterterpene from an *Ircinia* marine sponge. *J. Org. Chem.* **1985**, *50*, 284–286.

35. Kimura, J.; Ishizuka, E.; Nakao, Y.; Yoshida, W.Y.; Scheuer, P.J.; Kelly-Borges, M. Isolation of 1-methylherbipoline salts of halisulfate-1 and of suvanine as serine protease inhibitors from a marine sponge, *Coscinoderma mathewsi*. *J. Nat. Prod.* **1998**, *61*, 248–250.
36. Di Leva, F.S.; Festa, C.; D'Amore, C.; de Marino, S.; Renga, B.; D'Auria, M.V.; Novellino, E.; Limongelli, V.; Zampella, A.; Fiorucci, S. Binding mechanism of the farnesoid X receptor marine antagonist suvanine reveals a strategy to forestall drug modulation on nuclear receptors. Design, synthesis, and biological evaluation of novel ligands. *J. Med. Chem.* **2013**, *56*, 4701–4717.
37. Cassiano, C.; Monti, M.C.; Festa, C.; Zampella, A.; Riccio, R.; Casapullo, A. Chemical proteomics reveals heat shock protein 60 to be the main cellular target of the marine bioactive sesterterpene suvanine. *ChemBioChem* **2012**, *13*, 1953–1958.
38. Singleton, M.R.; Dillingham, M.S.; Wigley, D.B. Structure and mechanism of helicases and nucleic acid translocases. *Annu. Rev. Biochem.* **2007**, *76*, 23–50.
39. Wang, C.-C.; Huang, Z.-S.; Chiang, P.-L.; Chen, C.-T.; Wu, H.-N. Analysis of the nucleoside triphosphatase, RNA triphosphatase, and unwinding activities of the helicase domain of dengue virus NS3 protein. *FEBS Lett.* **2009**, *583*, 691–696.
40. Ndjomou, J.; Kolli, R.; Mukherjee, S.; Shadrick, W.R.; Hanson, A.M.; Sweeney, N.L.; Bartczak, D.; Li, K.; Frankowski, K.J.; Schoenen, F.J.; *et al.* Fluorescent primuline derivatives inhibit hepatitis C virus NS3-catalyzed RNA unwinding, peptide hydrolysis and viral replicase formation. *Antivir. Res.* **2012**, *96*, 245–255.
41. Saalau-Bethell, S.M.; Woodhead, A.J.; Chessari, G.; Carr, M.G.; Coyle, J.; Graham, B.; Hiscock, S.D.; Murray, C.W.; Pathuri, P.; Rich, S.J.; *et al.* Discovery of an allosteric mechanism for the regulation of HCV NS3 protein function. *Nat. Chem. Biol.* **2012**, *8*, 920–925.
42. Ding, S.C.; Kohlway, A.S.; Pyle, A.M. Unmasking the active helicase conformation of nonstructural protein 3 from hepatitis C virus. *J. Virol.* **2011**, *85*, 4343–4353.
43. Tani, H.; Akimitsu, N.; Fujita, O.; Matsuda, Y.; Miyata, R.; Tsuneda, S.; Igarashi, M.; Sekiguchi, Y.; Noda, N. High-throughput screening assay of hepatitis C virus helicase inhibitors using fluorescence-quenching phenomenon. *Biochem. Biophys. Res. Commun.* **2009**, *379*, 1054–1059.
44. Copeland, R.A. *Evaluation of Enzyme Inhibitors in Drug Discovery*; John Wiley & Sons: New York, NY, USA, 2005; pp. 111–140.
45. Salam, K.A.; Furuta, A.; Noda, N.; Tsuneda, S.; Sekiguchi, Y.; Yamashita, A.; Moriishi, K.; Nakakoshi, M.; Tsubuki, M.; Tani, H.; *et al.* Inhibition of hepatitis C virus NS3 helicase by manoalide. *J. Nat. Prod.* **2012**, *75*, 650–654.
46. Salam, K.A.; Furuta, A.; Noda, N.; Tsuneda, S.; Sekiguchi, Y.; Yamashita, A.; Moriishi, K.; Nakakoshi, M.; Tsubuki, M.; Tani, H.; *et al.* Psammaplin A inhibits hepatitis C virus NS3 helicase. *J. Nat. Med.* **2013**, *67*, 765–772.
47. Takahashi, H.; Takahashi, C.; Moreland, N.J.; Chang, Y.-T.; Sawasaki, T.; Ryo, A.; Vasudevan, S.G.; Suzuki, Y.; Yamamoto, N. Establishment of a robust dengue virus NS3-NS5 binding assay for identification of protein-protein interaction inhibitors. *Antivir. Res.* **2012**, *96*, 305–314.

PLOS ONE

Binding of HSV-1 Glycoprotein K (gK) to Signal Peptide Peptidase (SPP) Is Required for Virus Infectivity

Sariah J. Allen[1], Kevin R. Mott[1], Yoshiharu Matsuura[2], Kohji Moriishi[3], Konstantin G. Kousoulas[4], Homayon Ghiasi[1]*

1 Center for Neurobiology and Vaccine Development, Ophthalmology Research, Department of Surgery, Los Angeles, California, United States of America, **2** Department of Molecular Virology, Research Institute for Microbial Diseases, Osaka University, Osaka, Japan, **3** Department of Microbiology, Faculty of Medicine Yamanashi University, Yamanashi, Japan, **4** Division of Biotechnology and Molecular Medicine, School of Veterinary Medicine, Louisiana State University, Baton Rouge, Louisiana, United States of America

Abstract

Glycoprotein K (gK) is a virion envelope protein of herpes simplex virus types 1 (HSV-1) and 2 (HSV-2), which plays important roles in virion entry, morphogenesis and egress. Two-hybrid and pull-down assays were utilized to demonstrate that gK and no other HSV-1 genes specifically binds to signal peptide peptidase (SPP), also known as minor histocompatibility antigen H13. SPP dominant negative mutants, shRNA against SPP significantly reduced HSV-1 replication *in vitro*. SPP also affected lysosomes and ER responses to HSV-1 infection. Thus, in this study we have shown for the first time that gK, despite its role in fusion and egress, is also involved in binding the cytoplasmic protein SPP. These results also suggest that SPP plays an important role in viral replication and possibly virus pathogenesis. This makes SPP unique in that its function appears to be required by the virus as no other protein can compensate its loss in terms of viral replication.

Citation: Allen SJ, Mott KR, Matsuura Y, Moriishi K, Kousoulas KG, et al. (2014) Binding of HSV-1 Glycoprotein K (gK) to Signal Peptide Peptidase (SPP) Is Required for Virus Infectivity. PLoS ONE 9(1): e85360. doi:10.1371/journal.pone.0085360

Editor: Deepak Shukla, University of Illinois at Chicago, United States of America

Received November 4, 2013; **Accepted** November 20, 2013; **Published** January 20, 2014

Funding: This work was supported by National Institutes of Health (NIH) grant 1 RO1 EY13615 to HG. KGK was supported by NIH AI43000 and NGMS P20 GM103458. The funders had no role in study design, data collection and analysis, decision to publish, or preparation of the manuscript.

Competing Interests: The authors have declared that no competing interests exist.

* E-mail: ghiasih@CSHS.org

Introduction

Signal peptide peptidase (SPP), also known as minor histocompatibility antigen H13, is an aspartyl protease member of the intramembrane cleaving proteases family (I-CLiP), which specializes in the cleavage of signal peptides after their release by signal peptidase (SP) [1,2]. SPP and SPP-like (SPPL) proteins are evolutionarily conserved in *H. sapiens*, *Rattus norvegicus*, *Oryza sativa japonica*, *B. subtilis*, *Gallus gallus*, *B. taurus*, *X. laevis*, *Macaca mulatta*, *D. rerio*, *D. melanogaster*, *C. elegans*, *S. pombe*, *A. thaliana*, *P. falciparum* [3–6] and there exists a 96% amino acid homology between human and mouse SPP [7]. SPP localizes predominantly to the endoplasmic reticulum (ER) and can exist in different forms depending on glycosylation status [8]. Unlike other family members, SPP appears to achieve enzyme activity in the absence of protein cofactors [1,9,10]. SPP has been shown to play important roles in extracellular and intracellular signaling events such as cellular surveillance in MHC-I signal peptide processing [2] and has been linked to pathogenic conditions such as Alzheimer's disease [11], certain cancers [12], and human cytomegalovirus, pestivirus, malaria and Hepatitis C infections [13–17].

HSV-1 infections are among the most frequent serious viral eye infections in the U.S. and are a major cause of viral-induced blindness [18–22]. HSV-1-induced corneal scarring (CS), also broadly referred to as herpes stromal keratitis (HSK), can lead to blindness; thus, HSV-1 is the leading cause of corneal blindness due to an infectious agent in developed countries [21,23,24]. In addition to necrotizing HSK, ocular infection with HSV-1 can cause eye disease ranging in severity from blepharitis, conjunctivitis, and dendritic keratitis, to disciform stromal edema [22,23,25–28]. In the U.S. approximately 500,000 people suffer recurrent ocular HSV episodes annually, requiring doctor visits, medication and corneal transplants in severe cases. Although the HSV-1 gene(s) which are involved in eye disease are presently unknown, we have demonstrated previously that immunization of mice with glycoprotein K (gK), but not with any other known HSV-1 glycoprotein, significantly exacerbates CS and facial dermatitis following ocular HSV-1 infection [29–32]. This exacerbation of CS occurs independently of both the virus strain used for infection and the strain of mouse studied [31]. gK is encoded by the UL53 open reading frame and is a highly hydrophobic 338-amino-acid protein with a predicted molecular mass of 37-kDa [32–34]. Both gK from HSV-1 and HSV-2 are 338 amino acids long with approximately 84% amino acid homology [33,35,36]. Genome wide screenings in both HSV-1 [37] and HSV-2 [38] have shown that gK elicited $CD8^+$ IFN-γ responses in mice and humans, respectively.

gK is an essential HSV-1 gene [32–34,39] and single amino acid changes within gK cause extensive virus-induced cell fusion [40–43]. Furthermore, gK is an important determinant of cytoplasmic virion envelopment, since viruses lacking gK fail to efficiently acquire a cytoplasmic envelope resulting in a drastic defect in virion morphogenesis, egress and spread [44–47]. Deletion of gK results in the formation of extremely rare microscopic plaques indicating that gK is required for efficient

virus replication [44,45,47,48], a concept that is supported by the observation that gK-deficient virus can only be propagated on complementing cells that express gK [44,45]. As gK is essential to HSV-1 infectivity, we had previously analyzed its contribution to CS using recombinant viruses (rather than deleting the *gK* gene) with two extra copies of *gK* and found that similar to gK immunization, this recombinant virus caused elevated levels of CS in both mice and rabbits [49]. We have also shown that an elevation of anti-gK antibody in individuals with a history of HSV-1 recurrence is correlated with increased severity of eye disease [50].

In this study we show for the first time that: 1) HSV-1 gK binds to SPP and 2) SPP is required for virus infectivity. Despite the seriousness of ocular herpes infection, no drug has been FDA approved for prevention of ocular recurrences. Thus, blocking SPP activity or binding to viral glycoproteins (such as gK) by targeted therapeutics may represent a clinically effective and expedient approach to the reduction of viral replication and the resulting pathology.

Materials and Methods

Cells and viruses

Vero and HeLa cells were obtained from American type culture collection (ATCC). RS (rabbit skin) cells (from Steven L Wechsler) was described previously [51]. HeLa and Vero cells were grown in DMEM media plus 10% fetal bovine serum (FBS), while RS cells were grown in MEM media plus 5% FBS, while. Triple plaque-purified HSV-1 strain McKrae was grown in RS cell monolayers as described previously [32]. V5-tagged gK recombinant viruses in KOS background (gKV5DI, gKV5DII, gKV5DIII, and gKV5DIV) were grown as described previously [52].

Two hybrid system

We performed a bacterial two-hybrid using the BacterioMatch Two-Hybrid System (Stratagene, La Jolla, CA) and a mouse brain plasmid cDNA library (Stratagene). The bait plasmid pBT expressing a λ repressor (λcI)-fused gK protein and the target plasmid pTRG expressing the α-subunit of RNA polymerase fused to cDNA library-encoded proteins were used in the study. We used an *E.coli* reporter strain containing the two reporter genes LacZ and Carbenecillin-resistance ($Carb^r$) under the control of the λcI/α-subunit of RNA polymerase. Additionally, the pBT plasmid, the pTRG plasmid and the *E.coli* reporter strain contained the chloroamphenicol (Cam^r), tetracycline (Tet^r) and kanamycin (Kan^r) resistance genes, respectively. To construct the pBT-gK, a cDNA encoding gK was amplified by polymerase chain reaction (PCR) using specific primers containing EcoRI/XhoI sites and inserted into the corresponding sites in the pBT bait plasmid. The mouse brain cDNA library was amplified, harvested and final plasmid DNA (pTRG-cDNA mouse brain library) purification conducted according to manufacturer's protocol. The *E.coli* reporter strain was transformed with pBT-gK and cDNA library cloned into pTRG and transformants were selected on Carb + Cam + Tet + Kan supplemented LB-Agar plates. The putative positive colonies were further tested for Lac Z activity by replica plating these clones onto X-gal indicator plates (Cam + Tet + Kan +X-gal + β-galactosidase inhibitor LB-Agar) followed by screening for the blue color indicative of Lac Z expression. The mouse brain library plasmids were recovered from the positive colonies and the inserted target cDNA was sequenced using pTRG plasmid-specific primers as described in the manufacture's protocols. NCBI-BLAST analysis [53] was performed on collected sequences and putative genes identified (Figure S1).

Construction and expression of c-myc-gK and HA-SPP

The gK and SPP constructs used in this study are shown in Figures S2 and S3, respectively. In Figure S2, a schematic diagram of full-length gK with an in-frame c-myc tag at the carboxy terminus is shown. Figure S3 shows a schematic diagram of full-length SPP with an in-frame HA tag and ER retention signal also located at the carboxy terminus as we described previously [16]. gK with c-myc tag was synthesized (GenScript, Piscataway, NJ) and inserted into BamHI site of pcDNA3.1 and sequences were verified with standard dideoxy sequencing at the UCLA Genotyping and Sequencing core. Amaxa nucleofactor kit R (Lonza, Allendale, NJ) was used to transfect 10^6 HeLa or Vero cells with plasmid DNA cocktail containing both HA-SPP and c-myc-gK in a ratio of 1:1 in accordance with manufacturer instruction. Protein expression was monitored over 5 days using Coomassie blue protein staining and Western blotting. Antibodies against HA and c-myc (GenScript), were diluted according to manufacturer instruction in the total Western HRP kit (GenScript). Optimum c-myc-gK and HA-SPP expression and recovery was determined to be 48–72 hr post-transfection.

Construction and expression of SPP shRNA constructs

shRNAs against SPP were created using the Knockout single vector inducible RNAi system (Clontech, Mountain View, CA). Briefly, SPP siRNA oligonucleotides were designed using siRNA-designer (www.clontech.com). The shRNAs chosen correspond to SPP nucleotide locations 409–430 (#5/6); 644–666 (#11/12); 1134–1157 (#19/20) and a scramble of #11/12. The four shRNA were synthesized and ligated into pSingle-tTS-shRNA (Invitrogen) via XhoI and MluI restriction sites and the sequence was verified using standard dideoxy sequencing. RS cells were grown to 70% confluency on Lab-Tex chamber slides (BD Falcon, San Jose, CA) and transfected with either SPP shRNA or scramble shRNA using Lipofectamine-2000 (Invitrogen, Carlsbad, CA) for 8 hr followed by addition of plasmid inducer doxycycline for 12 hr prior to HSV-1 infection according to manufacturer instruction. Cells were infected with 0.1 PFU of HSV-1 strain McKrae for 1 hr at 37°C, virus was then removed with three 1X PBS washes and normal growth media + shRNA inducer replaced for 2, 4, 6, 8, 20 or 40 hr post-infection (PI). At each time point virus titer was measured via standard plaque assay on RS cells as we described previously [31]. Briefly, 100 μL aliquots of 10-fold serial dilutions were placed on confluent monolayers of RS cells in 24-well plates, incubated at 37°C for 1 hr and overlaid with medium containing 1% methylcellulose. The plates were incubated at 37°C for 3 days and stained with 1% crystal violet, and the viral plaques were counted.

Construction and expression of SPP dominant negative mutants

We previously constructed two mutant forms of SPP in which enzymatically critical Asparagine residues were mutated to Alanine at positions 219 (D219A) and 265 (D265A) [16]. These dominant negatives are also HA tagged with ER-retention signals at the carboxy terminus in pcDNA3.1 vector as shown in Figure S3 and as we described previously [16]. RS cells were grown to confluency in Lab-Tex chamber slides and transfected with SPP-HA, D219A-HA or D265A-HA plasmids using Lipofectamine-2000 (Invitrogen). Transfection was allowed to proceed for 24 hr followed by infection with 0.1 PFU of HSV-1 strain McKrae as described above. Cells were grown for 12, 24 or 48 hr PI and HSV-1 titer measured by standard plaque assay on RS cells as described above.

Immuoprecipitation (IP)

HeLa or Vero cells were transfected with c-myc-gK and HA-SPP as described above and were harvested at 48 hr post-transfection. Cells were lysed with lysis buffer included in the Classic IP Kit (Pierce, Rockford, IL) and 600 µg cellular extract was incubated with Dynabeads-G (Invitrogen) which were pre-bound to either HA, c-myc, irrelevant His-antibody (Invitrogen) or SPP (Abcam) antibody. Incubation proceeded for 1 hr at RT and beads were washed 5X with lysis buffer followed by kit-supplied elution buffer and finally SDS-PAGE analysis and Western blotting using the reverse antibodies that was used for IP.

Colocalization and virus detection by immunocytochemistry (ICC)

HeLa, Vero and RS cells were grown to confluency on Lab-tek chamber slides and infected with gK-V5-DII recombinant HSV-1 for 24 hr as we described previously [52]. Infected cells were fixed with 4% paraformaldehyde for 1 hr at 4°C followed by 20 minutes incubation in serum free protein block (Dako, Carpentaria, CA) at room temperature. Rabbit anti-SPP (Abcam) was diluted according to manufacturer instructions and incubated on slides overnight at 4°C. Slides were then washed and incubated with anti-V5-FITC, anti-FITC Alexa Fluor 488 and anti-rabbit Alexa Fluor 594 (Invitrogen) for 1 hr at RT. Washed slides were air dried and mounted with 4′,6-diamidino-2-phenylindole (DAPI) prolong Gold (Invitrogen). The fluorophores were imaged in separate channels with a Zeiss ApoTome-equipped Axio Imager Z1 (Carl Zeiss Microimaging). For anti-HSV-1-gC-FITC staining, RS or Vero cells were grown to confluency on chamber slides and transfected with shRNA construct or dominative negative construct as described above, followed by infection with 0.1 PFU/cell of McKrae for 24 hr. Fixative, blocking and mounting was the same as above except with anti-HSV-1-gC-FITC antibody incubation at a 1:100 dilution overnight at 4°C (Genway, San Diego, CA). For organelle straining, RS cells were grown to confluency on chamber slides and transfected with shRNA as described above followed by infection with 0.1 PFU/cell of McKrae for 24 hr. Fixative, blocking and mounting was the same as above except with rabbit polyclonal antibodies (Abcam) against LAMP (ab24170), EEA1 (ab2900) or Calnexin (ab22595) diluted according to manufacturer instruction followed by anti-rabbit Alexa Fluor 594 secondary antibody at 1:200 dilution.

Fluorescent-activated cell sorting (FACS)

RS cells were transfected with SPP shRNA 11/12 as above followed by infection with 0.1 PFU/cell of HSV-1 strain McKrae for 24 hr or mock-infected. Infected or mock-infected cells were harvested via centrifugation and stained with annexin-V PE mAb (eBioscience, San Diego, CA). Stained cells were washed 2X with FACS buffer (1X PBS with 0.1% sodium azide), resuspended in 4% paraformaldehyde, and analyzed using a multicolor five-laser LSR II instrument (Applied Biosystems, Foster City, CA).

Gene expression analyses

qRT-PCR was performed as follows: at various times post infection, total RNA was extracted, and 1,000 ng of total RNA was reverse transcribed as we have described previously [54]. The differences in the expression levels of mRNAs were evaluated using custom-made TaqMan gene expression primers against ICP0, tK, gB and gK with optimized primer and probe concentrations (Applied Biosystems). Primer probe sets consisted of two unlabeled PCR primers and the FAM^{TM} dye-labeled TaqMan MGB probe formulated into a single mixture. Additionally, all cellular amplicons included an intron-exon junction to eliminate signal from genomic DNA contamination. The assays used in this study were as follows: 1) gB specific primers (forward, 5′-AACGCGACGCACATCAAG-3′; Reverse - 5′-CTGGTACGCGATCAGAAAGC-3′; and Probe - 5′-FAM-CAGCCGCAGTACTACC-3′). Amplicon Length = 72 bp; 2) ICP0 specific primers (forward, 5′- CGGACACG-GAACTGTTCGA-3′; reverse, 5′-CGCCCCCGCAACTG-3′; and probe, 5′-FAM-CCCCATCCACGCCCTG-3′). Amplicon length = 111 bp; 3) TK specific primers (forward, 5′- CAG-TAGCGTGGGCATTTTCTG-3′; reverse primer, 5′-CCTCGCCGGCAACAAAA-3′; and probe, 5′-FAM-CTCCAGGCGGACTTC-3′). Amplicon length = 59 bp; and 4) gK specific primers (forward, 5′-GGCCACCTACCTCTT-GAACTAC-3′; reverse primer, 5′-CAGGCGGG-TAATTTTCGTGTAG-3′; and probe, 5′-FAM-CAGGCCG-CATCGTATC-3′). Amplicon length = 82 bp. As an internal control, a set of GAPDH primers from Applied Biosystems (ASSAY I.D. m999999.15_G1 – Amplicon Length = 107 bp) was used.

In some experiments the relative copy numbers for ICP-0, gB, and gK expressions were calculated using standard curves generated from the plasmids pGem-ICP0, pAc-gB1, and pAC-gK1, while in other experiments of ICP-0, tk, gB, and gK expressions were normalized to the levels present 1 hr after virus is first added to the cell monolayer (the adsorption period), a time is routinely taken as t = 0. In all experiments, GAPDH was used for normalization of transcripts. qRT-PCR was performed using an ABI ViiA7 sequence detection system (Applied Biosystems) in 384-well plates. The threshold cycle (CT) values, which represent the PCR cycles at which there is a noticeable increase in the reporter fluorescence above baseline, were determined using ViiA7 RUO software.

Results

HSV-1 gK binds to SPP

We hypothesized that gK might exert its previously demonstrated pathogenic functions via interactions with one or more cellular proteins. Briefly, we performed a two-hybrid screening assay using the BacterioMatch Two-Hybrid System (Stratagene, San Diego, CA). In this assay, gK was used as a bait to probe a mouse brain cDNA library to find cellular proteins that interact with gK. A total of 1×10^6 independent cDNA clones were screened and upon sequencing we observed a significant homology to all isoforms of SSP (Fig. S1) suggesting a possible interaction of gK and SPP.

To confirm the bacterial two-hybrid result of gK binding to SPP, we first used a pull-down approach. Cellular extracts from HeLa cells transiently expressing HA-SPP, c-myc-gK or both plasmids were immunoprecipitated using protein G beads bound to either anti-myc, anti-HA, or the irrelevant anti-His antibody. Immunoprecipitates were subjected to Western analysis to detect c-myc-gK (using c-myc Ab) or HA-SPP (using HA Ab). We created the tagged myc-gK plasmid as there is no commercially available antibody against gK. Furthermore, we have previously failed in attempts to make antibody against either full-length gK or gK peptide fragments in multiple hosts (mouse, rabbit and chicken). Figure 1A demonstrates pull-down of HA-SPP by anti-HA antibody, while Figure 1B demonstrates pull-down of c-myc-gK by anti-c-myc antibody demonstrating that both proteins can be individually immunoprecipitated using this system. Figures 1C and 1D demonstrate successful co-immunoprecipitation of HA-SPP and c-myc-gK in two cell lines. Figure 1C shows gK-SPP

interaction via both pull-down of c-myc-gK by anti-HA immunoprecipitation and pull-down of HA-SPP by anti-c-myc immunoprecipitation in HeLa cells. Neither HA-SPP nor c-myc-gK were pulled down in untransfected HeLa cells (lane 1 in each figure), or by irrelevant His-antibody (data not shown). Our HeLa cell co-immunoprecipitation results were also confirmed in Vero cells (Fig. 1D). These experiments confirm our two-hybrid analysis and further suggest that gK can bind to SPP *in vitro*.

It is possible that SPP could bind to other HSV-1 proteins and thus our result would not be an interaction specific to gK. To address this possibility we performed an additional IP with RS cells that had been infected with 0.1 and 1.0 PFU/cell of HSV-1 strain McKrae to probe for interaction of other viral proteins with SPP. At 24 hr PI, infected cells were subjected to IP using SPP antibody or total anti-HSV-1 antibody with mock serum as a control. This anti-HSV-1 antibody recognizes many HSV-1 genes including all major HSV-1 glycoproteins (i.e., gB, gC, gD) but not gK. The results demonstrate that the total anti-HSV-1 antibody was able to pull down many HSV-1 proteins, but not SPP (not shown). In addition, the IP against SPP was not able to pull down any HSV-1 reacting proteins (not shown). Taken together these data demonstrate that gK is the only HSV-1 gene that binds to SPP *in vitro*.

Virus-expressed gK colocalizes with cellular SPP *in vitro*

To explore if gK and cellular SPP co-localize within the HSV-1 infected cells, HeLa, Vero and RS cells were infected with four different HSV-1 recombinant viruses expressing V5 in-frame in each of the four proposed domains of gK (Figure 2) [52]. These recombinant viruses differ in the placement of the V5 tag; DI and DIV have V5 on the luminal side while DII and DIII have the tag on the cytoplasmic side (Figure 2G). Cells were infected with each virus individually and IHC was performed using antibodies against SPP and V5 as described in Materials and Methods. We detected strong colocalization between V5-gK and endogenous SPP with DI (Figure 2A), DII (Figure 2B) and DIII (Figure 2C) infected RS cells. In contrast, HeLa and Vero cells had the strongest colocalization with only DII and DIII viruses (Figures 2B and 2C), while we observed minor colocalization with the DIV virus in

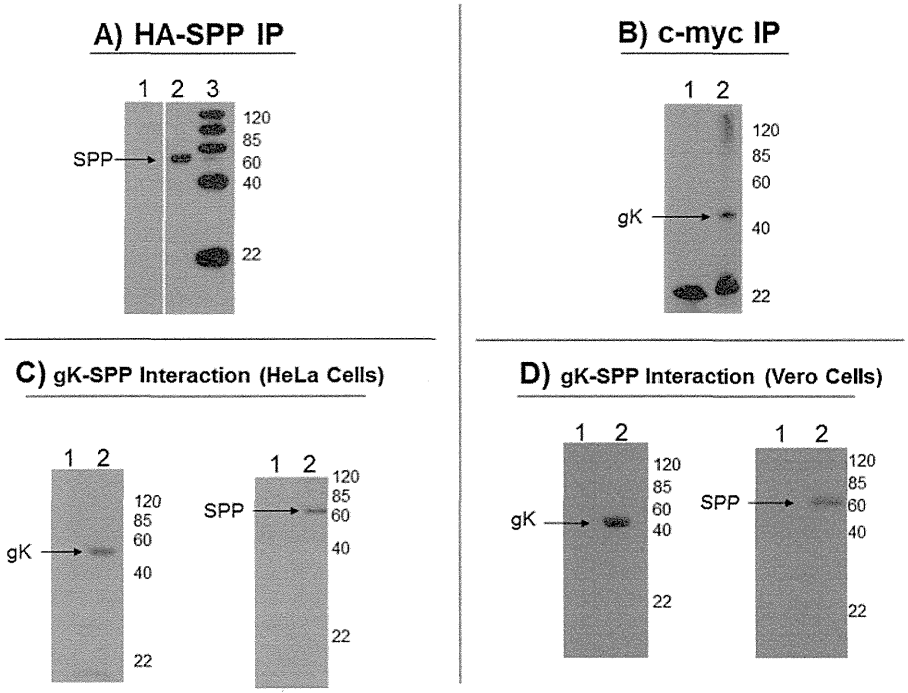

Figure 1. Binding of gK to SPP *in vitro*. HeLa cells were transfected with c-myc-gK and HA-SPP plasmids at a 1:1 ratio for 48 hr. A) Expression and pull-down of HA-SPP. Cellular lysates were incubated with anti-HA antibody bound to IgG beads and the resulting IP was subjected to Western blot analysis with anti-HA antibody. Lane 1 shows untransfected HeLa cells and no HA-SPP band, while Lane 2 shows HA-SPP correctly immunoprecipitating from transfected lysates. Lane 3 is protein size marker; B) Expression and pull-down of c-myc-gK. Cellular lysates were incubated with anti-c-myc antibody bound to IgG beads and the resulting IP was subjected to Western blot analysis with anti-c-myc antibody. Lane 1 shows untransfected HeLa cells no c-myc-gK band, while Lane 2 shows c-myc-gK correctly immunoprecipitating from transfected lysates. Protein sizes are indicated; and C/D) Co-immunoprecipitation of gK and SPP; C) HeLa Cells. Left panel: Cellular lysates were incubated with anti-HA antibody bound to IgG beads and the resulting IP was subjected to Western blot analysis with anti-c-myc antibody. Lane 1 shows untransfected HeLa cells and no gK band, while Lane 2 shows a successful pull-down of gK by anti-HA antibody. Right panel: Cellular lysates were incubated with anti-c-myc antibody bound to IgG beads and the resulting IP was subjected to Western blot analysis with anti-HA antibody. Lane 1 shows untransfected HeLa cells and no SPP band, while Lane 2 shows a successful pull-down of SPP by c-myc-gK. Protein sizes are indicated; D) Vero Cells. Left panel: Cellular lysates were incubated with anti-HA antibody bound to IgG beads and the resulting IP was subjected to Western blot analysis with anti-c-myc antibody. Lane 1 shows untransfected Vero cells and no gK band, while Lane 2 shows a successful pull-down of gK by anti-HA antibody. Right panel: Cellular lysates were incubated with anti-c-myc antibody bound to IgG beads and the resulting IP was subjected to Western blot analysis with anti-HA antibody. Lane 1 shows untransfected Vero cells and no SPP band, while Lane 2 shows a successful pull-down of SPP by c-myc-gK; E) HSV-1 infected lysates subjected to IP with total HSV-1 serum followed by Western blot with total HSV-1 serum pulled down many proteins; F) HSV-1 Infected lysates subjected to IP with total HSV-1 serum followed by Western blot with anti- SPP antibody did not pull down SPP; and G) HSV-1 infected lysates subjected to IP with anti-SPP antibody followed by Western blot with total HSV-1 serum did not pull down any HSV-1 reacting proteins. Protein sizes are indicated.

doi:10.1371/journal.pone.0085360.g001

all cells lines tested (Figure 2D) and no colocalization in uninfected control cells (Figure 2E). The gK-SPP interaction in all cell lines infected with the 4 recombinant viruses are quantified and shown in Figure 2F. These results validate our immunoprecipitation results, since cellular SPP and HSV-1 expressed gK colocalize within the cell.

SPP shRNA reduces HSV-1 replication *in vitro*

It has been previously shown that small interfering RNA targeted to SPP reduced the production of infectious HCV particles [55]. To explore the possibility that a reduction in SPP production would effect HSV-1 replication, we constructed three shRNA plasmids against SPP as described in Materials and Methods. In a pilot experiment we tested the efficacy of these shRNA against HSV-1 replication *in vitro*, and determined that shRNA construct 11/12 was the most potent in reducing SPP expression in Vero, RS, and HeLa cell lines (Figure S4). We next tested this shRNA construct in RS cells to determine if SPP knockdown had any effect on HSV-1 viral replication. Cells were transfected with SPP shRNA, followed by infection with 0.1 PFU of HSV-1 strain McKrae and HSV-1 titer was measured by standard plaque assays. After 8 hr PI the SPP shRNA plasmid began to significantly reduce viral replication *in vitro* when compared to scrambled SPP shRNA plasmid (Fig 3A). Thus, these results suggest that SPP is needed for efficient HSV-1 infectivity.

During the course of primary HSV-1 infection, gene expression is synchronized in a cascade fashion. Thus, to determine if the observed reduction in virus replication described above (Fig. 3A) affected different classes of HSV-1 gene expression, we investigated the effect of SPP inhibition on HSV-1 tk, gB, and gK expression at various times PI. RS cells were transfected with shRNA plasmids followed by infection with HSV-1 strain McKrae as described above. qRT-PCR was performed on total RNA isolated from transfected-infected RS cells and real time analysis performed. We detected significant reductions in expression of tk, gB, and gK from 2.5 to 20 hr in cells treated with SPP shRNA compared to cells treated with control scramble shRNA (Fig 3B). These results indicate that tk and gB expression is also impaired when SPP expression is blocked.

To confirm our titration and gene expression studies, we next performed ICC against HSV-1 during treatment with shRNA against SPP. RS cells were transfected and infected as above, and at 24 hr PI subjected to ICC using anti-HSV-1-gC antibody. We observed reduced staining for HSV-1 in SPP shRNA transfected RS cells compared to scramble shRNA control (Fig. 3C). We also observed a much more confluent monolayer in SPP shRNA transfected and infected cells indicating reduced cellular lysis as compared to SPP scramble shRNA transfected and infected cells. To demonstrate that the reduction in viral replication and gene expression was not due to higher apoptosis, we performed qRT-PCR on RS cells transfected with SPP shRNA and infected with HSV-1 and compared it to RS cells infected with HSV-1 alone

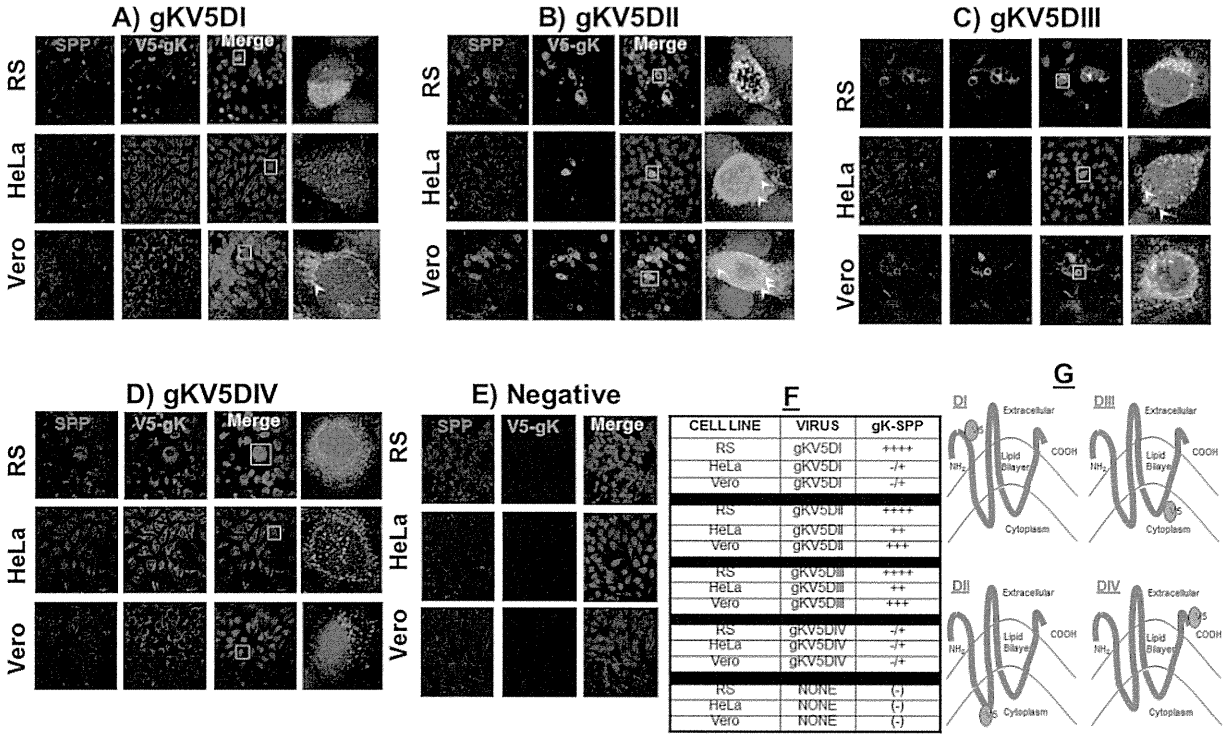

Figure 2. gK colocalizes with SPP *in vitro*. HeLa, Vero and RS cells were infected with 100 PFU/cell of each of four different recombinant HSV-1 expressing V5 tagged gK. Infection was allowed to proceed for 24 hr and slides were fixed, blocked and stained with mouse-anti-V5-FITC (green), rabbit-anti-SPP-TRITC (red) and DAPI nuclear stain (blue). Photomicrographs are shown at 40X direct magnification and colocalization was visualized as yellow. Panels: A) HeLa, Vero and RS cells were infected with gKV5DI; B) HeLa, Vero and RS cells were infected with gKV5DII; C) HeLa, Vero and RS cells were infected with gKV5DIII; D) HeLa, Vero and RS cells were infected with gKV5DIV; E) Mock-infected HeLa, Vero and RS cells; F) Qualitative assessment of colocalization of V5-gK and SPP in all cell lines; and G) V5-gK constructs showing the domain location of the V5 tag within the gK protein. Arrows point to less obvious areas of colocalization. In each panel the top cell line is RS cells, the middle panel is HeLa cells and the bottom panel is Vero cells.
doi:10.1371/journal.pone.0085360.g002

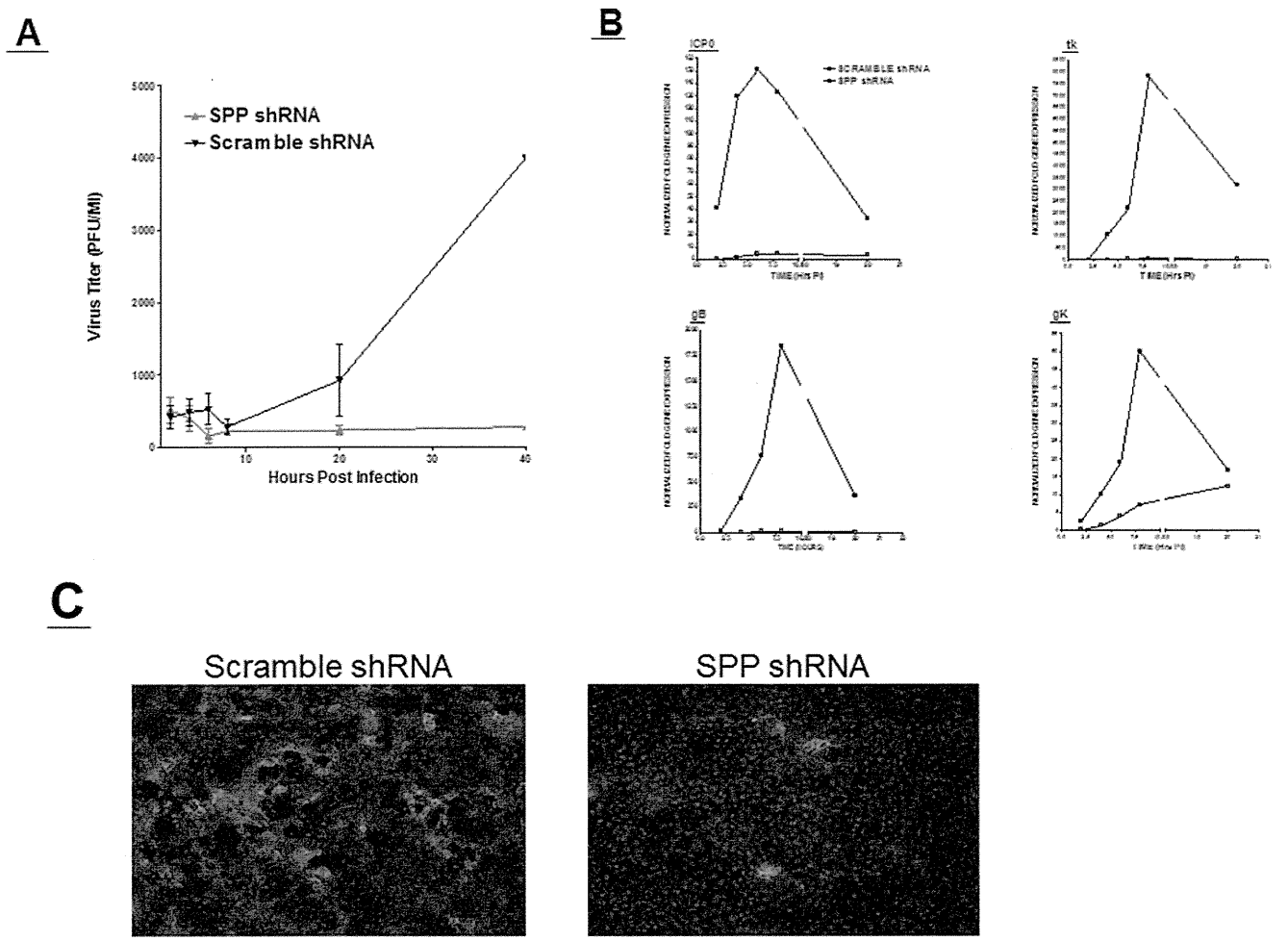

Figure 3. Blocking HSV-1 replication *in vitro* by SPP shRNA. A) Viral Titer is reduced by SPP knockdown. RS cells were transfected for 24 hr with either SPP shRNA or scramble shRNA and infected with 0.1 PFU/cell of HSV-1 strain McKrae. Titers were measured by standard plaque assays at 2.5, 5, 7.5, 10, 20 and 40 hr PI. Each point represents the mean ± SEM from 3 independent experiments per time point; B) HSV-1 gene expression is reduced by SPP knockdown. RS cells were transfected and infected as above. Transfected and infected cells were harvested 2, 4, 6, 8 and 20 hr PI, RNA extracted and cDNA synthesized. Expression of tk, gB and gK were measured using qRT-PCR and each point represents the mean ± SEM from 3 independent experiments; and C) HSV-1 protein expression is reduced by SPP knockdown. RS cells were transfected and infected as in A for 24 hr PI. Cells were stained with anti-HSV-1-gC-FITC (green) and costained with DAPI (blue). Photomicrographs are shown at 10X magnification.
doi:10.1371/journal.pone.0085360.g003

and mock-treated control cells. We observed a significant reduction in apoptosis in the presence of the SPP shRNA plasmid compared to cells infected with HSV-1 alone (Figure S5). This suggests that shRNA against SPP is not increasing cell death and is actually protective of HSV-1 induced apoptosis. Taken together, our RNA interference studies suggest that SPP is required for efficient HSV-1 infectivity.

The effect of blocking SPP on intercellular transport properties of the HSV-1 in the ER, lysosomes and endosomes was evaluated in HSV-1 infected RS cells. RS cells were transfected with SPP shRNA or scramble shRNA followed by infection with HSV-1. Transfected-infected cells were monitored by immunofluorescence or immunocytochemistry for the effect of SPP shRNA on morphological properties of the ER, lysosomes and endosomes. We detected significant differences between infected cells in presence of SPP shRNA compared with cells transfected with scramble shRNA and infected which were similar to uninfected cells (Fig. 4A). Loss of SPP function resulted in the loss of discrete punctate structures representing the endosomes around the nuclear rim. RS cells were also infected with V5-tagged gK recombinant virus gKV5DIII. Double staining for V5-gK and ER is shown in Figure 4B, the arrow indicates a HSV-1 infected cell. Our results show that gK also localizes in the ER (yellow), which marks the primary site for a direct interaction between gK and SPP.

With regards to endosomes we did not detect differences between mock infected control and infected cells treated with SPP shRNA or scramble shRNA (Fig. 5). However, we detected striking difference in the lysosomes between mock infected control and infected cells treated with SPP shRNA compared with cells transfected with scramble shRNA and infected with HSV-1 (Fig. 5). In cells transfected with scramble shRNA and infected, lysosomes were less visible upon infection and mostly located around the nuclear rim and near the ER. Upon shRNA downregulation of SPP the lysosomal population becomes very similar to the uninfected cells. In this latter case the lysosomes were uniformly distributed in the cytoplasm. Thus, our results suggest that SPP regulates lysosomes and ER in response to HSV-1 infection.

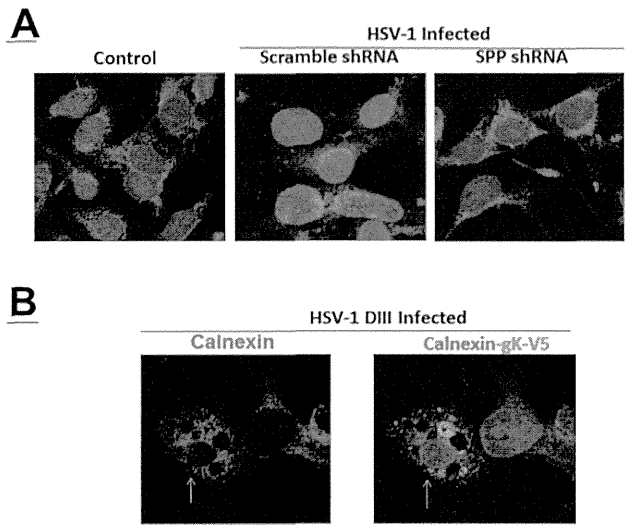

Figure 4. HSV-1 induces ER morphology changes which can be blocked by SPP shRNA. A) RS cells were grown to confluency on chamber slides and transfected with SPP shRNA or scramble shRNA followed by infection with 1 PFU/cell of HSV-1. At 24 hr PI, slides were fixed, blocked and stained with rabbit-anti-calnexin-TRITC (red) and DAPI nuclear stain (blue). Photomicrographs are shown at 40X direct magnification. HSV-1 infection induces condensation of ER while treatment with SPP shRNA restores normal ER morphology. B) RS cells were infected with gKV5DIII and stained for V5 (green) and calnexin (red). Arrow indicates HSV-1 infected cell.
doi:10.1371/journal.pone.0085360.g004

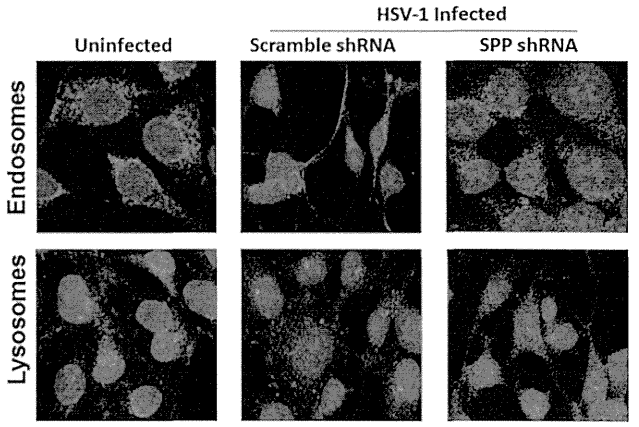

Figure 5. Effect of blockage of gK interaction with SPP on intercellular transport properties of the HSV-1 in the lysosome and endosome. RS cells were grown to confluency on chamber slides and transfected with SPP shRNA or scramble shRNA followed by infection with 1 PFU/cell of HSV-1. At 24 hr PI, slides were fixed, blocked and stained with rabbit-anti-EEA1-TRITC (red) for endosome or rabbit-anti-LAMP-TRITC (red) for lysosome. DAPI was used for nuclear staining (blue). Photomicrographs are shown at 40X direct magnification.
doi:10.1371/journal.pone.0085360.g005

SPP dominant negative mutants reduce HSV-1 replication *in vitro*

Dominant negative mutants are a powerful tool for studying enzyme function as they complex with endogenous proteins, inactivating the wild-type cellular proteins within the same cell. The active site mutants, Asp219 (D219A) and Asp265 (D265A) (constructs shown in Fig. S3), in which the catalytic aspartate residues are mutated to alanine, have been shown to be dominant negative inhibitors of endogenous SPP activity [1,56]. These catalytic aspartates are highly conserved in all aspartic proteases and their mutation destroys proper coordination of a water molecule in the enzymatic active site, thereby destroying the acid-base reaction and rendering the mutants unable to catalyze their substrate. Importantly, these mutations do not affect substrate binding. To determine if the effect of these dominant negative mutants would confirm our shRNA results, RS cells were transfected with mammalian expression plasmids containing HA-tagged dominant negative SPP plasmids, D219A or D265A, followed by infection with 0.1 PFU of HSV-1 strain McKrae. The kinetics of virus replication were quantitated by determining the amount of infectious virus at various times PI using a standard plaque assay as described in Materials and Methods. Replication of HSV-1 in cells transfected with D219A or D265A was significantly lower than the control group at various times PI (Fig. 6A). In addition, D265A blocked virus replication more efficiently then D219A (Fig. 6A). These results are consistent with our shRNA results (Fig. 3, above) demonstrating that blocking SPP catalytic ability, but not substrate binding, significantly reduces HSV-1 virus replication *in vitro*.

To confirm our titration results with dominant negative mutants, we transfected and infected monolayers of RS and Vero cells as above and subjected them to ICC with anti-HSV-1-gC antibody. Representative photomicrographs of infected RS cells (Fig. 6B, top panels) and Vero cells (Fig. 6C, bottom panel) are shown. In both RS and Vero cells, the presence of D219A and D265A reduced the amount of HSV-1 positive cells compared with control groups (Fig. 6B and C). The positive cells per slide were quantitated and indicate that there is approximately a 10 fold reduction in HSV-1 signal in cells transfected with SPP dominant negative mutants compared to untreated control cells (Fig 6D). Collectively, these results confirm that reducing functional SPP impairs HSV-1 replication.

Discussion

Herein, we show for the first time that SPP is required for HSV-1 infectivity and that SPP specifically binds to gK. Similar to this study, it was previously shown that small interfering RNA targeted to SPP reduced the production of infectious HCV particles [55]. In this study by using SPP dominant negative constructs and SPP shRNA we have demonstrated that SPP is indeed essential for viral replication. gK has been shown to interact with both HSV-1 gB and UL20 [57,58]. However, our pull-down involving gK expressing plasmid rules out the possibility that the gK-SPP interaction is strictly dependent upon complexing with other viral proteins. Furthermore, our pull-down of HSV-1 infected RS cells using total HSV-1 antibody which does not recognize gK failed to precipitate SPP and vice versa.

The role of SPP in the context of HSV-1 infection has yet to be elucidated; however HSV-1 gK is a type III transmembrane protein which contains an N terminal signal sequence utilized for its insertion into the membrane [59,60]. HSV-1 gK has also been shown to traffic through both the trans-Golgi network (TGN) [52] and the rough endoplasmic reticulum (RER) [46]. To date, all identified SPP substrates are signal peptides which span the ER in a type II topology [2,61]. However, to our knowledge there is no study showing that SPP cannot catabolize type III membrane proteins. Type III membranes differ from type II in being multi-pass with the targeting signal sequence on the amino terminus. The location of the signal sequence within gK is essential as both deletion of the N terminus and N terminal cleavage via protease reduce HSV-1 virion entry [62]. Recent work suggests that despite